

# DETECTION AND RETRIEVAL OF CYSTS IN JOINT ULTRASOUND B-MODE AND ELASTICITY BREAST IMAGES

Jingdan Zhang<sup>1</sup>, Shaohua Kevin Zhou<sup>1</sup>, Shelby Brunke<sup>2</sup>, Carol Lowery<sup>2</sup>, and Dorin Comaniciu<sup>1</sup>

<sup>1</sup>Robust Analysis and Content Retrieval Program, Siemens Corporate Research, Princeton, NJ, USA

<sup>2</sup>Ultrasound Division, Siemens Healthcare Sector, Issaquah, WA, USA

## ABSTRACT

Distinguishing cysts from other tumors is a routine clinical practice for diagnosing breast cancer. It has shown that more accurate diagnosis can be achieved by combining elasticity images with traditional B-mode ultrasound images [1]. In this paper, we propose a *fully automatic* system to detect cysts jointly in both B-mode and elasticity images. It is based on database-guided techniques that learn the knowledge of cyst appearance automatically from B-mode and elasticity images in a database. Further, for a detected cyst in a query image, the cysts with similar image appearance in the database are retrieved to improve diagnostic accuracy and confidence. In the experiment, we show that our system achieves high sensitivity and specificity in cyst diagnosis.

**Index Terms**— breast cyst detection and retrieval, ultrasound (US) imaging, elasticity imaging

## 1. INTRODUCTION

Ultrasonography is widely used in diagnosing diseases due to its low cost, portability, and low risk to patients. In the case of breast cancer diagnosis, it is a complimentary technique to mammography [2]. Ultrasonography shows unique value in distinguishing benign tumors from malignant ones in clinical studies [3, 4]. However, traditional B-mode ultrasound imaging has good sensitivity but poor specificity in diagnosing malignant tumors due to insufficient information in B-mode images [5].

Elasticity imaging (EI) is an emerging ultrasound technique measuring spatial variation of the elastic modulus of tissue. Unlike B-mode images, which describe composition properties of tissue by capturing backscatter acoustic information, EI images describe mechanical properties by capturing relative tissue stiffness and hardness. Because tumors are usually stiffer than surrounding tissues, EI images provide useful information to breast cancer diagnosis [6].

EI images are especially valuable for distinguishing cysts, which are usually benign, from other tumors. Figure 1 compares the appearance of cysts (the first and the second row) to the appearance of non-cyst tumors (the third row). In Figure 1, images are shown in registered pairs, each of which consists of a B-mode breast image and its corresponding EI image. Cysts are visible in B-mode images; but their appearance in B-mode is not distinctive enough to differentiate them from other tumors. EI images supplement additional information for diagnosing cysts [1]. For a cyst in EI, there is usually a black ring at the middle and a posterior brightening at the bottom. Combining the information from both B-mode and EI leads to more reliable cyst diagnosis.

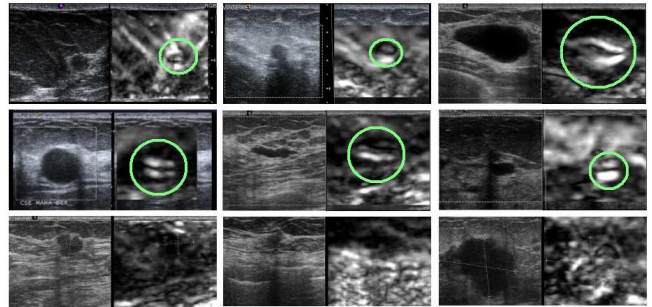


**Fig. 1.** The appearance of cysts and non-cyst tumors in both B-mode and EI images. The first and the second row show cyst images. The third row shows images without cyst. The cysts in EI are highlighted by circles.

In this paper, we propose a computer-aided diagnosis (CAD) system for automatically detecting breast cysts in registered B-mode and EI ultrasound images and retrieving similar cases from a database. The system is based on database-guided techniques. Prior knowledge of cyst appearance is learned from a medical database with expert annotations for distinguishing cysts from their background and other tumors. We use information jointly from B-mode and EI in cyst detection to achieve a high detection accuracy. In order to improve the diagnostic confidence, given a detected cyst, the cysts with similar image appearance in the database are retrieved. The image similarity is computed robustly based on the detection probability. The proposed system could improve the accuracy of the breast cyst diagnosis and reduce the labor cost.

Database-guided techniques have been successfully applied to detect the left ventricle in 2D echocardiograms [7] and heart chambers in 3D CT images [8]. However, the previous approaches only use information from one image modality in detection. Our system uses information from both B-mode and EI images. Also in these previous systems, the main purpose of automatic detection is to save labor cost. Retrieving similar cases in the database is not a requirement.

Content-based image retrieval (CBIR) has been one of the most active research areas in the field of computer vision [9]. It has a lot of important applications in medical imaging as reviewed in [10]. In [11], an image retrieval technique is proposed to classify breast tumors as benign or malignant lesions based on regions-of-interest (ROI) indicated manually by physicians. Our system automatically determines ROI and computes image similarity using the detection probability.

Section 2 elaborates the proposed fully automatic detection algorithm and the retrieval similarity measurement. Section 3 presents

This research was done when Carol Lowery was an employee at Siemens.

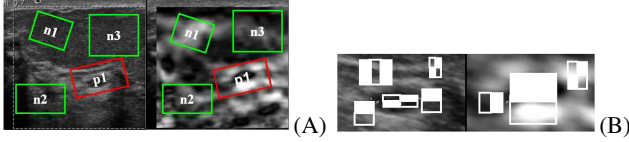


**Fig. 2.** (A) The positive (red) and negative (green) training examples collected from an image pair. Two patches with a same label belong to a pair. (B) A pair of image patches extracted from (A). The feature candidates are from both B-mode and EI image patches.

our experimental results. Section 4 concludes the paper.

## 2. METHODS

In this section, we first present the detail for the cyst detection algorithm that localizes the cyst jointly in B-mode and EI images and then address how to perform cyst retrieval from a database of images.

### 2.1. Cyst detection

#### Problem formulation

In data acquisition, a B-mode and an EI image are captured as a registered pair  $I = (I_{Bmode}, I_{EI})$ . The location of a cyst in the image pair is defined by a bounding box, described by five parameters  $\alpha = (x, y, \theta, w, h)$ , where  $(x, y)$  is the center of the box,  $w$  and  $h$  are the width and height of the box, and  $\theta$  is the orientation.

The purpose of cyst detection is to automatically determine the cyst location  $\alpha$  in a given image pair  $I$ . This can be cast as computing the conditional probability  $p(\alpha|I)$ , where  $p(\alpha|I)$  describes the probability of a cyst present at a hypothetical location  $\alpha$  in the image pair  $I$ . We further formulate cyst detection as a two-class classification problem (cyst is +1 and the background and other tumors are -1) and learn a classifier in a database-guided manner to compute  $p(\alpha|I)$ :

$$p(\alpha|I) \propto P(+1|\tau(I, \alpha)) \quad (1)$$

where  $\tau(I, \alpha) = (\tau(I_{Bmode}, \alpha), \tau(I_{EI}, \alpha))$  is a pair of image patch defined by the bounding box  $\alpha$  in the image pair  $I$  and  $P(+1|\tau(I, \alpha))$  represents the probability of  $\tau(I, \alpha)$  being a cyst. Next we show how to learn the probability  $p(\alpha|I)$  using an annotated database and how to use it to detect cysts in unseen images.

#### Offline training

We first collect a database of B-mode and EI image pairs. In order to robustly discriminate between cyst and non-cyst patterns, the database includes both image pairs with cysts, as shown in the first and second row of Figure 1, and pairs without cyst, as shown in the third row of Figure 1. In the database, the bounding boxes of cysts are annotated by experts.

We then sample positive and negative examples from the database. A training example is a pair of image patches  $\tau(I, \alpha)$  as shown in Figure 2(B). If the bounding box  $\alpha$  contains a cyst, it is a positive training example. Otherwise, it is a negative. Figure 2(A) shows several training examples sampled from a pair of cyst images. When there is no cyst in an image pair, all examples collected from the pair are negatives.

Given a training example, a pool of Haar-like features [12] are extracted to represent image information. Haar-like features can be efficiently evaluated using integral images [12]. By varying the parameters of these features, we can obtain a large number of feature candidates. In order to represent information in B-mode and EI, the

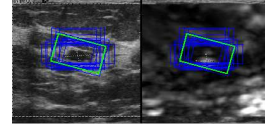


**Fig. 3.** The initial detection result (the blue boxes) and the aggregated result (the green box).

features are computed from both image patches, as shown in Figure 2(B).

We use probabilistic boosting tree (PBT) [13] to train a classifier for differentiating the positive examples from the negatives. Other learning techniques such as probabilistic boosting network [14] can be used too. PBT combines a set of Adaboost classifiers [15] to a tree structure. When training each tree node, Adaboost iteratively selects features that mostly decrease the classification error rate. By providing feature candidates from both B-mode and EI images, the information from these two image modalities is automatically leveraged by the PBT classifier.

#### Online testing

Given a new image pair, cysts are detected by exhaustively scanning all possible bounding boxes in the images. PBT computes the probability  $P(+1|\tau(I, \alpha))$  by integrating the probabilities obtained at its nodes. Usually, there are multiple detections with high probabilities around the ground truth, as shown in Figure 3. We aggregate these overlapping boxes to one box by averaging their position, scale, and orientations. The confidence of the aggregated box  $\alpha$  containing a cyst is defined as:

$$\Phi(\alpha) = \sum_{\alpha' \in N(\alpha)} P(+1|\tau(I, \alpha')), \quad (2)$$

where  $N(\alpha)$  is a set of bounding boxes which overlap with the box  $\alpha$  at a ratio larger than a predefined value. The probabilities of these boxes are summed to obtain a robust measurement of confidence.

We control the specificity and sensitivity of the cyst detection by defining a confidence threshold  $\lambda$ . If  $\Phi(\alpha) > \lambda$ , we consider the box  $\alpha$  contains a cyst. Otherwise, there is no cyst in the box. The detector will have a high sensitivity and low specificity when the threshold  $\lambda$  is set to a small value and vice versa.

### 2.2. Cyst Retrieval

After cyst detection, we retrieve similar cases from the database based on the cyst content to provide more evidence for diagnosis. This can be achieved by defining a similarity function between two cyst pairs. How to define a meaningful similarity measurement between two images is a non-trivial problem. In literature, a variety of similarity measurements have been proposed [9, 10, 11]. For example, in [11], the similarity between two image patches containing breast tumors is computed based on the Euclidean distance of the auto-covariance features extracted from the two patches.

For our application, we are more interested in the appearance similarity between cysts. Thus, we directly use image intensity of a cyst as its feature vector and measure the similarity of two cysts using the normalized cross correlation of the two feature vectors:

$$C(\tau(J, \alpha_J), \tau(I, \alpha_I)) = \left\langle \frac{V(\tau(J, \alpha_J))}{\|V(\tau(J, \alpha_J))\|}, \frac{V(\tau(I, \alpha_I))}{\|V(\tau(I, \alpha_I))\|} \right\rangle \quad (3)$$

where  $\tau(J, \alpha_J)$  and  $\tau(I, \alpha_I)$  are two cyst image patches normalized to a predefined image size,  $V(\tau(J, \alpha_J))$  and  $V(\tau(I, \alpha_I))$  are

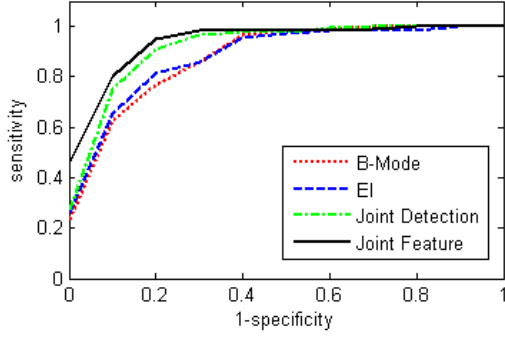


**Fig. 4.** The ROC curves of the four detection approaches. The x-axis is 1-specificity and the y-axis is sensitivity.

vectors obtained by concatenating the pixel intensity values of the corresponding patches, and  $\langle \circ, \circ \rangle$  is the inner product of two vectors.

We apply Principal Component Analysis (PCA) [16] to reduce the cost of computing the similarity function. In training, a projection matrix is computed based on the feature vectors of the cyst images in the database. When computing (3), feature vectors are projected to a low dimensional space, which captures the major variation of the feature vector. The robustness of the similarity computation is also improved due to reduction of noise energy in projection.

When retrieving similar cases after the cyst detection, the final aggregated result can be used to compute the similarity. However, the similarity computed in this way is susceptible to the detection error even when the aggregated result is close to the ground truth. In order to improve the robustness of the similarity measurement, we integrate the cyst similarity of the detected cyst candidate boxes in a query image  $I$  to a reference image  $J$ , weighted by their probability of being a cyst:

$$\Omega(\tau(J, \alpha_J), \tau(I, \alpha_I)) = \sum_{\alpha' \in N(\alpha_I)} C(\tau(J, \alpha_J), \tau(I, \alpha')) p(\alpha' | I) \quad (4)$$

where  $J$  is a cyst pair in database,  $\alpha_J$  is the expert annotation,  $\alpha_I$  is the aggregated final detection result, and  $N(\alpha)$  is a set of boxes used for aggregation. This reduces the effect of the detection error to the final retrieval results.

### 3. RESULTS

The performance of the cyst detection and retrieval was tested on a database of B-mode and EI pairs. We collected 57 cyst image pairs and 61 non-cyst pairs captured by Siemens Ultrasound machines. The cyst locations in the cyst pairs are annotated by experts.

#### 3.1. Results on cyst detection

We conducted threefold cross-validation to test the detection performance, in which we partitioned the data into three sets and we run three benchmarks. Each data set has 1/3 cyst pairs and 1/3 non cyst pairs. In a benchmark, we select a set as the test set and the remaining two sets as the training set. The overall performance was computed as the average of the three benchmarks.

In testing, if an aggregated detection box overlaps with the ground truth box in a large portion, it is considered as a correct detection. Otherwise, it is a wrong one. We computed the sensitivity

| Specificity (%) | sensitivity (%) |       |            |               |
|-----------------|-----------------|-------|------------|---------------|
|                 | B-mode          | EI    | Joint Det. | Joint Feature |
| 75.0%           | 81.9%           | 82.8% | 95.8%      | <b>97.1%</b>  |
| 80.0%           | 79.1%           | 80.4% | 92.5%      | <b>96.1%</b>  |
| 85.0%           | 69.8%           | 77.4% | 87.2%      | <b>93.6%</b>  |
| 90.0%           | 61.4%           | 72.8% | 74.6%      | <b>78.9%</b>  |
| 95.0%           | 48.2%           | 59.6% | 57.9%      | <b>63.2%</b>  |

**Table 1.** The specificity and sensitivity of the four detection approaches.

and specificity of cyst detection as:

$$\text{sensitivity} = \frac{\text{Num. of True Pos.}}{\text{Num. of True Pos.} + \text{Num. of False Neg.}} \quad (5)$$

$$\text{specificity} = \frac{\text{Num. of True Neg.}}{\text{Num. of True Neg.} + \text{Num. of False Pos.}} \quad (6)$$

In order to show the benefit of using features from B-mode and EI jointly, we trained and tested the classifier in four approaches:

1. B-mode classifier, which only uses B-mode features in training and testing;
2. EI classifier, which only uses EI features in training and testing;
3. Joint detection, which uses the B-mode and EI classifiers trained in (1) and (2) in testing. The detected boxes are jointly aggregated from the boxes detected by the two classifiers; and
4. Joint feature, which is proposed in Section 2.1.

We adjusted the confidence threshold  $\lambda$  to plot the receiver operating characteristic (ROC) curves of the detectors, as shown in Figure 4. Table 1 lists the sensitivity values of the four approaches with same specificity value. We can observe that B-mode or EI image alone does not provide sufficient evidence to discriminate cysts from their background and other tumors. Aggregating B-mode and EI detection results provides better performance. Our approach has *consistently* recorded the best performance by training only one classifier that uses B-mode and EI features jointly. Figure 5 shows some detection results.

#### 3.2. Results on cyst retrieval

After cyst detection, similar cases were retrieved from the database. Given a detected cyst, we sorted all cases in the database based on the similarity measurement defined in Equation (4). Figure 6 shows two detection and retrieval results. For each detection, the two most similar and the two least similar cases in the database are presented. As shown in the figure, the visually similar cases were successfully retrieved.

### 4. CONCLUSIONS

In this paper, we have presented a CAD system for automatically detecting breast cysts in registered B-mode and EI ultrasound images. Our system is based on database-guided techniques which learn the knowledge of cyst appearance from a cyst image database. We have proposed a joint detection approach, using information from both B-mode and EI images at a feature level. We have demonstrated that the joint feature-based detection approach outperforms detection approaches based on a single modality or the joint detector approach. In order to improve the diagnostic confidence, we have proposed a robust similarity function to retrieve similar cysts in the database based on the detection result.

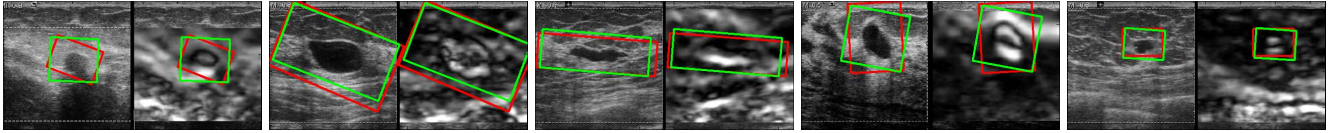


**Fig. 5.** Some cyst detection results. The ground truths are red boxes. The detection results are green boxes.

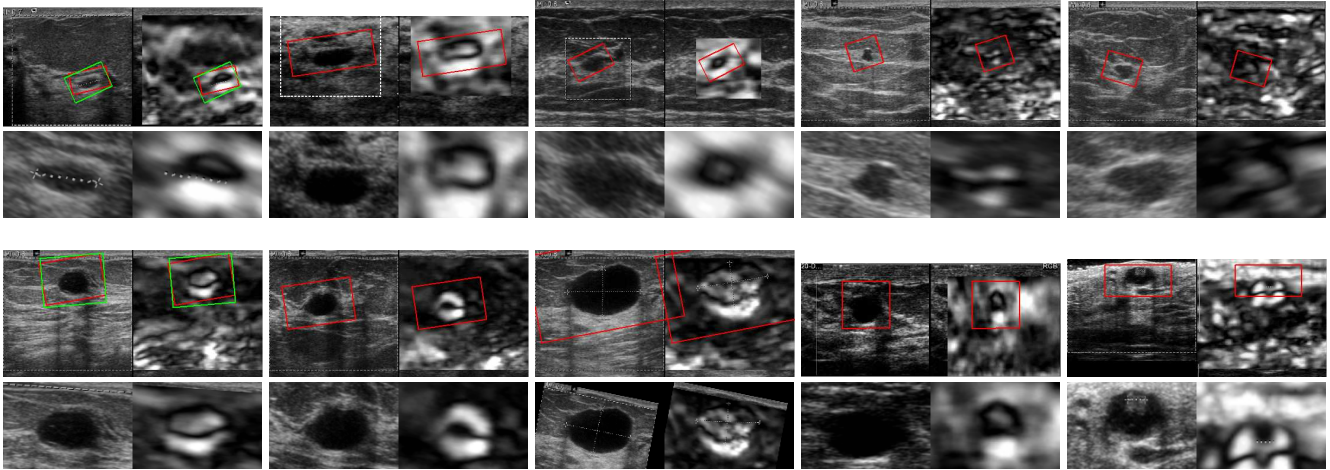


**Fig. 6.** Two cyst detection and retrieval results. The first column shows the two detection results and the image patches cropped from the detected boxes. The second and third column show two cases in the database that are most similar to the detection results. The cyst image patches are cropped from the ground truth boxes. The fourth and fifth column show the two least similar cases.

## 5. REFERENCES

- [1] W. A. Berg and et al., "Combined screening with ultrasound and mammography vs mammography alone in women at elevated risk of breast cancer," *The Journal of American Medical Association*, vol. 299(18), pp. 2151–2163, 2008.
- [2] A. M. Bosch and et al., "Interexamination variation of whole breast ultrasound," *British Journal of Radiology*, vol. 76, pp. 328–331, 2003.
- [3] P.M. Shankar, J.M. Reid, H. Ortega, C.W. Piccoli, and B.B. Goldberg, "Use of non-rayleigh statistics for identification of tumors in ultrasonic B-scans of the breast," *IEEE Trans. Medical Imaging*, vol. 12(4), pp. 687–692, 1993.
- [4] AT Stavros, D Thickman, CL Rapp, MA Dennis, SH Parker, and GA Sisney, "Solid breast nodules: Use of sonography to distinguish between benign and malignant lesions," *Radiology*, vol. 196, pp. 122–134, 1995.
- [5] E. Warner and et al., "Surveillance of brca1 and brca2 mutation carriers with magnetic resonance imaging, ultrasound, mammography, and clinical breast examination," *The Journal of American Medical Association*, vol. 292(11), pp. 1317–1325, 2004.
- [6] B. Garra, E. Cespedes, J. Ophir, S. Spratt, R. Zurbier, C. Magnant, and M. Pennanen, "Elastography of breast lesions: initial clinical results," *Radiology*, vol. 202, pp. 79–86, 1997.
- [7] B. Georgescu, X. S. Zhou, D. Comaniciu, and A. Gupta, "Database-guided segmentation of anatomical structures with complex appearance," in *CVPR*, 2005.
- [8] Y. Zheng, A. Barbu, B. Georgescu, M. Scheuering, and D. Comaniciu, "Fast automatic heart chamber segmentation from 3D ct data using marginal space learning and steerable features," in *ICCV*, 2007.
- [9] R. Datta, D. Joshi, J. Li, and J.Z. Wang, "Image retrieval: Ideas, influences, and trends of the new age," *ACM Comput. Surv.*, vol. 40, no. 2, pp. 1–60, 2008.
- [10] H. Müller, N. Michoux, D. Bandon, and A. Geissbuhler, "A review of content-based image retrieval systems in medical applications - clinical benefits and future directions," *International J. of Medical Informatics*, vol. 73, no. 1, pp. 1–23, 2003.
- [11] Y.L. Huang, D.R. Chen, and Y.K. Liu, "Breast cancer diagnosis using image retrieval for different ultrasonic systems," in *Proc. IEEE ICIP*, 2004.
- [12] P. Viola and M. Jones, "Rapid object detection using a boosted cascade of simple features," in *Proc. CVPR*, 2001.
- [13] Z. Tu, "Probabilistic boosting-tree: Learning discriminative models for classification, recognition, and clustering," in *ICCV*, 2005.
- [14] J. Zhang, S.K. Zhou, L. McMillan, and D. Comaniciu, "Joint real-time object detection and pose estimation using probabilistic boosting network," in *CVPR*, 2007.
- [15] Y. Freund and R. Schapire, "A decision-theoretic generalization of online learning and an application to boosting," *J. Computer and System Sciences*, vol. 55, no. 1, pp. 119–139, 1997.
- [16] U. Sinha and H. Kangaroo, "Principal component analysis for content-based image retrieval," *RadioGraphics*, vol. 22, no. 5, pp. 1271–1289, 2002.